Journal of Seismic Response Control Systems, Vol. 1, pp. 25 – 50, 2025
https://doi.org/10.65423/h3kwag90

Effect of Boundary Conditions on Buckling Restrained Braced Frame Seismic Performance

Pratiksha Dhakal
Virginia Tech, USA.

Luis Ibarra
University of Utah, USA.
luis.ibarra@utah.edu

Received: 25 April 2025. **Accepted**: 22 October 2025. **Published**: 26 November 2025

Abstract

This study evaluates the effect of gusset plate behavior on the seismic performance of Buckling Restrained Braced Frames (BRBFs). The expected failure mode of these frames is yielding of the Buckling Restrained Brace (BRB) core, and although other BRB-related failure mechanisms are commonly reported, the performance and potential failure of BRB-gusset connections are rarely addressed. In this study, finite element (FE) models of BRBFs with diagonally-oriented BRBs braces were first calibrated in the nonlinear interval using the results of experimental BRBFs subjected to quasi-static cyclic loading. The tested specimens consisted of two BRBFs with different unbraced top gusset lengths, each one with two different beam connections (continuous and spliced beams). The calibrated FE models were then used to predict BRBF performance up to failure, considering monotonic loading. Thereafter, a parametric study assess the effect of several gusset plate parameters on the BRBF capacity. The evaluated parameters included the size, thickness, and initial imperfection of the gusset plate, as well as the presence of lug stiffeners. The study shows that cruciform lug stiffeners enhance the buckling capacity of gusset plates by more than 50% because BRB end plates in the out-of-plane (OOP) direction significantly reduce displacements in this direction at the gusset plate free end. The results indicate that the effective length factor used in analytical equations needs to be increased for frames with BRBs without cruciform lug plates. In addition, large gusset plate imperfections and thinner plates decrease the buckling capacity and may even modify the critical failure mode, but design practices and imperfection limits imposed by current codes and standards should prevent a significant decrease in BRBF capacity.

Keywords: Steel Frame; Buckling Restrained Braces; Gusset Plates; OOP Buckling; Abaqus; Finite Element Modeling.

1. Introduction

Buckling Restrained Braces (BRBs) have a steel core with a fully constrained yielding region and a reduced constant area – where the inelastic response is expected to produce uniform plastic strain along the yielding length (Andrews et al. 2008). As a result, the BRB achieves a compressive strength that often exceeds its tensile strength due to friction mechanisms, leading to asymmetrical and stable hysteresis behavior (Black et al. 2004, Kersting et al. 2015). However, other BRB failure modes have been reported, such as BRB global buckling, core local buckling, and restrainer local failure. The BRB performance is also affected by the interaction with the surrounding frame elements and the bracing connection (Okazaki 2012, Mahin et al. 2004, Roeder et al. 2006, Chou and Chen 2009, Wang et al. 2017). Because BRBs can undergo yielding under compression rather than buckling, Buckling Restrained Brace Frame (BRBF) gusset plates are subjected to higher compression forces than gussets of conventional braced frames. Under these heightened loads BRBF gusset plates may experience undesirable failure modes such as yielding, buckling, fracture, and failure of beam-column-gusset connection. Additionally, frame action demands may increase in braced frames at larger story drifts (Muir and Thornton, 2015), although some studies have found frame action effect is negligible when computing the BRBF buckling capacity (Chou and Liu 2012, Westeneng et al., 2015).

Current design procedures (e.g., AISC, 2016) treat gusset plates as axially loaded members, using Whitmore cross-section, defined by the plate thickness and Whitmore width. This approach calculates the buckling capacity of gusset plates in a similar fashion as prismatic columns; thus, requiring an effective length factor, K, and an equivalent length (Thornton, 1984). Dowswell (2006) proposed effective length factors for gusset plate design based on previous FE models and experimental tests. He grouped corner rectangular gussets into “compact” and “non-compact”, based on the gusset's stiffness and connection configuration. Dowswell reported a low variability in the capacity of compact plates, concluding that yielding is the applicable limit state for these plates and that buckling capacity computation is not necessary. However, Chou et al. (2012) tested a portal BRBF with a single-diagonal BRB under cyclic loading and found that gusset connections with no free-edge stiffeners exhibited a side-sway mode of gusset buckling, and proposed an effective length factor $K = 2.0$. Lin et al. (2005) studied the effect of adding stiffeners in gusset plates using FE modeling, concluding that stiffeners along the gusset free edge prevent out-of-plane (OOP) instability of the brace-to-column connections. For computing buckling based on the Whitmore and Thornton approaches, they recommended $K = 2.0$ instead of 0.65, for gussets with no free edge stiffeners. They concluded that stiffeners increase the rotational stiffness of the brace to gusset connection and increase the flexural demand on the BRBs. Along these lines, Westeneng et al. (2017) found that K may be larger than 2.0, depending on the gusset plate flexural stiffness.

To prevent OOP gusset failure, some researchers proposed gusset stiffeners. For instance, Chou and Liu (2012) performed a cyclic quasi-static test on a portal BRBF, using free edge stiffeners in gusset plates, finding BRB end plates yielded at an interstory drift of 1.5%. For similar BRBFs with gusset plates with no edge stiffeners, the top gusset plate buckled at an interstory drift of only 0.63%, and at an axial force less than the BRB compression strength. Tsai et al. (2008) conducted pseudo-dynamic and cyclic tests of a full-scale three-story three-bay BRBF with concrete-filled tube columns. They observed OOP buckling of the

first-story gusset plate at relatively low peak ground accelerations (PGAs). Free edge stiffeners were then added to the gusset plate, which changed the failure mode to buckling of the BRB core. Some of these experimental tests have reported additional BRBF failure modes, such as gusset-beam-column connection weld fracture in continuous beams (Chou and Liu, 2012; Lin et al., 2005).

The BRBF buckling capacity may significantly decrease if the BRB end plate-gusset connection acts as a pin in the OOP direction, an undesired condition that can be caused by BRB design characteristics. For instance, Okazaki et al. (2012) tested two chevron-configured BRBFs in a shake table, using BRBs with different embedment lengths. The frames were identical, but one of them included a BRB with an embedment length of less than 1.5-2.0 times the core projection's depth (see Takeuchi et al., 2008). Both frames had similar early responses, but for larger motions, the BRB with smaller embedment length behaved as a pin in the OOP direction – exhibiting significant damage – and leading to higher story drift and residual drifts. Numerical studies have also found that BRBF capacity can be limited by undesirable connection-related failures. For instance, Wigle and Fahnestock (2010) modeled 12 four-story BRBFs with varying brace end connection types (i.e., bolted, pinned, or welded), beam end conditions (continuous or spliced), and gusset plate thicknesses. They observed that thinner gusset plates had larger and more evenly distributed plate stresses than the diagonal zone of concentrated stresses found in thicker plates.

In summary, studies on the behavior of BRBFs show different types of failure and often contradicting results – in part because the effects of several parameters affecting the behavior of the BRB boundary conditions (BCs) are commonly excluded from the evaluation. For instance, the stiffness of the BRB lug plates in the OOP direction is not considered in any of the above studies. Also, gusset plate design is based on methodologies heavily dependent on the plate's unbraced length and effective length factor, two parameters that include several simplifications. This study investigates the effect of corner gusset plate behavior on the performance of BRBFs using FE prototypes modeled in the software ABAQUS (Dassault Systems, 2019), and subjected to monotonic loading up to failure of the frame components. Since modeling of framing members incorporates the frame action on a corner gusset plate (Williams and Richard 1996), all the BRBF components were modeled. The evaluated BRBF numerical models were subjected to monotonic loading up to the failure limit state. The models were validated and calibrated using on experimental tests of single bay frames. After the FE models were calibrated, parametric studies were performed to identify the main parameters controlling the BRBF failure modes.

2. Methodology

2.1. Experimental frames

Several experimental portal BRBFs were subjected to quasi-static cyclic loading protocols to obtain the envelope of the hyteresis loops and identify component damage, especially to the gusset plates (Ibarra, 2017; Dhakal, 2021). Therefore, the gusset and connections were not overdesigned; instead, the demand-to-capacity ratios for most components were kept slightly under unity. The portal frame represented the first floor of a four-story single braced bay frame design, heavily influenced by the AISC (2010) BRBF example prototype (Dhakal, 2021). The 3:4 scaled portal frame had a bay width base of 272 mm (10.88 ft)

and a height of 268 mm (10.56 ft) (Figure 1). The full-scale and scaled structures' members were selected to best match each other based upon demand-to-capacity ratios.

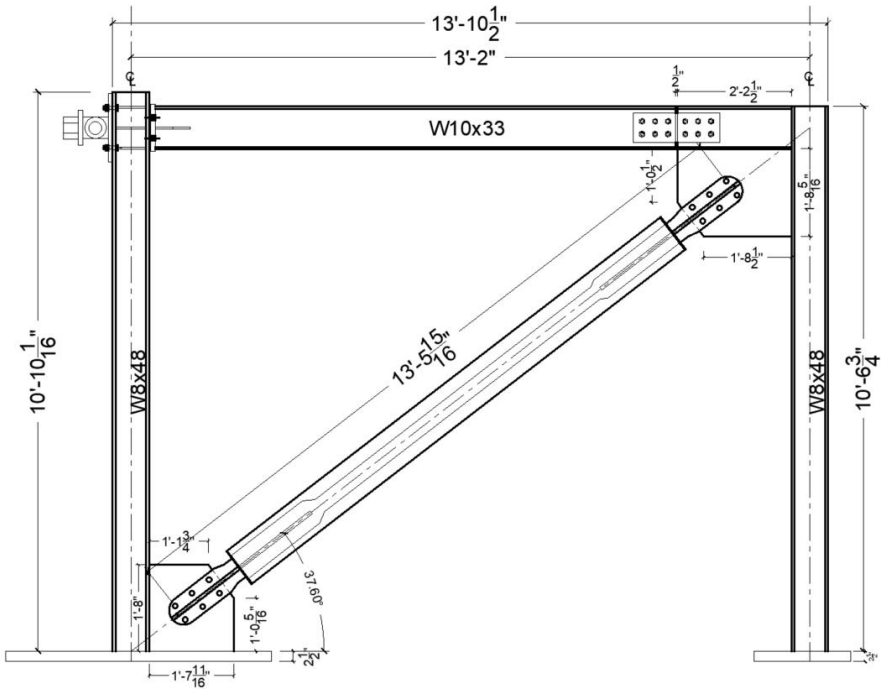

Figure 1. Sectional Elevation of Experimental Frame Setup.

Four BRBF setups were tested using two identical steel frames, except for the top gusset plate configuration. Frame 1 had a small top gusset plate (Figure 2a) with an average unbraced length $l_{avg} = 5.5$ in. (139.7 mm), according to the definition provided in Section 2.2. Note that the bottom gusset plate in both steel frames also had an average unbraced length $l_{avg} = 5.5$ in. Frame 2 had a large top gusset (Figure 2b) with an $l_{avg} = 10.5$ in. (266.7 mm), which was almost twice the l_{avg} of the top gusset plate in Frame 1, and close to the upper limit for compact plates.

Each steel frame was first tested as a hinged BRBF with articulation in the beam (Frames 1a and 2a, Table 1). These two frame setups were subjected to quasi-static cyclic loading protocols as per the AISC (2016) until the onset of yielding was detected in the gusset plates. Then, a continuous beam connection was created by adding plates to the top and bottom beam flanges at the splice location (Frames 1b and 2b, Table 1). The BRBFs with continuous beams were subjected to the same loading protocol, but this time loads were expected to be applied up to BRBF failure. Unfortunately, the actuator only reached a maximum compression load of 830.8 kN (187.0 kips) for both frames, without indication of imminent failure, despite the large initial imperfection in the case of Frame 2b.

A high seismic hazard was considered for the frame design. The design basis earthquake (DBE) short period acceleration was $S_{DS} = 1.0$ g, and for the 1.0 s. period the acceleration was $S_{D1} = 0.44$ g. The base shear

seismic coefficient was $C_S = 0.095$. The expected brace compression strength was computed as (AISC, 2016):

$$P_{BRB} = 1.1\beta\omega A_{BRB} F_{y,BRB} \quad (1)$$

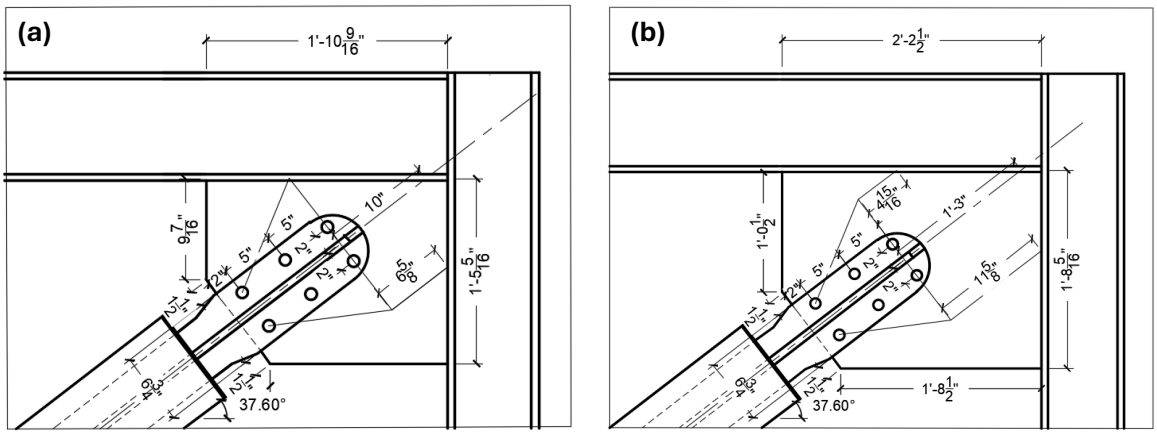

Figure ¡Error! No hay texto con el estilo especificado en el documento.. Gusset Plates in the Experiment. (a) Small Top Gusset Plate (b) Large Top Gusset Plate.

According to Equation 1, the BRB compression strength is P_{BRB}= 977 kN (220.0 kips), if the conservative coefficient of 1.1 for connection is not included. This calculation considers a BRB core area $A_{BRB} = 2258.1$ mm^2 (3.5 in^2), $F_{y,BRB} = 290$ MPa (42 ksi), as well as bolted-type BRB overstrength factors for tension (ω) and compression (β) of 1.36 and 1.1, respectively (Daniels 2011). The frame beam and columns in the FE model consisted of A992 steel sections W10×33 and W8×48, respectively. The gussets plates were A572 Grade 50, with a thickness $t_g = 9.525$ mm (3/8 in.). The modulus of elasticity (E) and Poison's ratio (υ) for all steel materials were 200,000 MPa (29,000 ksi) and 0.3, respectively.

2.2. Gusset plate design

The buckling stress gusset plate design followed AISC (2016) guidelines, which treat the gusset plate as a rectangular column plate spanning from the brace end to the framing members. To find a conservative allowable compression stress, Thornton (1984) proposed to use the unbraced central length l_1 as the gusset unbraced length (Figure 3), and to assume a fixed-fixed column condition with $K = 0.65$. The method was considered conservative because i) it ignores plate action, ii) it does not account for post-buckling strength of plates, and iii) the strip length is taken as the maximum unsupported length of the plate between the Whitmore Section and the supported edges of the plate. Thornton (1984) also mentioned that the average length, $l_{avg} = (l_1 + l_2 + l_3)/3$ (Figure 3) appears to give a more reasonable approximation of buckling strength, a conclusion supported by Dowswell's (2012) study, and recommended in AISC (2016).

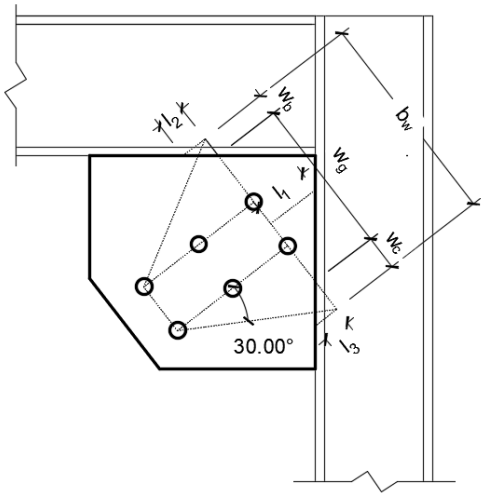

Figure 3. Whitmore Widths Occurring in Beam, Gusset, and Column.

The AISC specification for flexural buckling of columns was followed in this study. In all cases, the expected buckling failure mode is inelastic, given that the gusset plates always meet the inequality

$$KL/r \leq 4.71\sqrt{\frac{E}{F_{y,g}}} \tag{2}$$

where the length L is l_{avg}, r is the radius of gyration, and $F_{y,g}$ is the yield stress. Then, the critical buckling stress, F_{cr}, was determined as (AISC 2016):

$$F_{cr} = \left[0.658^{\frac{F_{y,g}}{F_e}}\right] F_{y,g} \tag{3}$$

In Eqn. 3, F_e is the elastic buckling stress computed with Euler's formula

$$F_e = \frac{\pi^2 E}{\left(KL/r\right)^2} \tag{4}$$

To compute the critical buckling load, P_{cr}, the area of the Whitmore section, A_w, is first calculated as:

$$A_w = w_g t_g + w_b t_{w,b} \frac{F_{y,bc}}{F_{y,g}} + w_c t_{w,c} \frac{F_{y,bc}}{F_{y,g}} \tag{5}$$

where w_g, w_b, and w_c are the Whitmore widths occurring in the gusset, beam, and column, respectively (Figure 3); whereas t_g, t_b, and t_c are the thickness of the gusset, beam, and column, respectively. Also, $F_{y,bc}$ is the yield stress of the gusset and beam-column elements. Based on these calculations, the critical buckling load, P_{cr}, was computed as:

$$P_{cr} = F_{cr} A_w \tag{6}$$

As observed, the gusset plate buckling capacity calculations are highly dependent on the gusset unbraced length and effective length factor, two parameters that include critical simplifications. Regarding the effective length factor, Thornton (1984) proposed $K = 0.65$, which is the AISC recommended value for a column with a fixed-fixed end condition. Dowswell (2006) developed a similar methodology for buckling capacity, based on the gusset plate classification. He considered a section compact if the gusset plate thickness is larger than the threshold thickness t_β:

$$t_g \geq t_\beta = 1.5 \sqrt{\frac{F_{y,g} c^3}{E l_1}} \tag{7}$$

where c is the shorter of the two perpendicular distances from the connected edge of the plate to the brace connection. For non-compact corner gussets, where $t_g < t_\beta$, Dowswell observed large discrepancies in the experimental versus anticipated buckling strength and used $K = 1.0$ and l_{avg}. The use of this larger K factor resulted in a conservative gusset plate buckling capacity that, on average, is about three times smaller than that reported from experimental tests. The $K = 1.0$ factor was a consequence of the large variability observed on non-compact plates. For compact plates, Dowswell concluded that the applicable limit state is yielding and that buckling capacity calculation is not needed. A combination of these methods has been implemented for BRBF gusset plate design in AISC, although Dowswell's and Thornton's studies focused on gusset plates of conventional braces, which are not subjected to large compression forces.

Table 1 summarizes the main characteristics of the gusset plates used in the four experimental tests. The small and large top gusset plates had an average unbraced length $l_{avg} = 139.7$ mm (5.5 in.) and 266.7 mm (10.5 in.), respectively. Both gusset plates meet Dowswell's (2006) compactness criterion, given that $t_g \geq t_\beta$ (see Eqn. 7). The Dowswell compactness criterion in Table 1 shows that Frames 1a and 1b (small top gusset) easily comply with this compact plate requirement. In contrast, the large top gusset plates of Frames 2a and 2b represent the upper limit of the compactness criteria – barely meeting the thickness required by the large gusset to be considered compact plates. Note, however, that once Dowswell's criterion of Eqn. 7 is satisfied, the gusset capacity does not need to be computed, and it is assumed that P_{BRB} controls the design.

Table 1 also compares Thornton's unfactored gusset plate buckling capacity (assuming $K = 0.65$, and l_{avg}), with respect to the BRB capacity, P_{BRB}, computed with Eqn. 1. For Frames 1a and 1b, the critical buckling load of the gusset plates using Thornton's method, $P_{cr,T}$, is about 20% larger than P_{BRB} and failure is expected on the BRB. For Frames 2a and 2b, $P_{cr,T}$ is about 1% smaller than P_{BRB}, and gusset failure marginally controls in this scenario. Note that according to Dowswell's method, both gusset plates are compact and their buckling capacity does not even need to be computed. Nevertheless, the $P_{cr,T}$ for the large gusset plate is slightly smaller than P_{BRB}, even when using non-conservative parameters in Thornton's

method (i.e., $K = 0.65$ and l_{avg}). Also observe that gusset capacity was the same for frames with hinge and continuous beams because frame action is not included in the formulation.

The method proposed by Sheng et al. (2002) was also used to predict P_{cr}, but the outcomes were even more conservative than those obtained from Thornton's method with $K = 0.65$ and l_{avg} (Dhakal, 2021). The modifications proposed by Chou et al. (2012) and Tsai (2005) to Thornton's method were even more conservative, as they proposed K values of 1.2 and 2.0, respectively. There are other comprehensive methods to assess gusset plate behavior (e.g., Zaboli et al. 2018, Takeuchi et al. 2014), but this study focus on the evaluation of the analytical method recommended in AISC using FE modeling.

Table 1. Gusset Plate Capacity for the Two Steel Frame Configurations.

Frame	Plate	Beam	l_1 mm (in.)	l_{avg} mm (in.)	Dowswell t_g vs t_β, mm (in.) *	Thornton $P_{cr,T}$ vs P_{BRB}, kN (kips) ǂ
1a	Small	Hinge	254 (10.0)	139.7 (5.5)	9.53 > 4.80 (0.375 > 0.189)	1201 > 977 (270 > 220)
1b	Small	Cont.	254 (10.0)	139.7 (5.5)	9.53 > 4.80 (0.375 > 0.189	1201 > 977 (270 > 220)
2a	Large	Hinge	381 (15.0)	266.7 (10.5)	9.53 > 8.51 (0.375 > 0.335)	970 < 977 (218 < 220)
2b	Large	Cont.	381 (15.0)	266.7 (10.5)	9.53 > 8.51 (0.375 > 0.335)	970 < 977 (218 < 220)

* If $t_g \geq t_\beta$ the plate is compact and the gusset plate capacity does not need to be computed.
ǂ $P_{cr,T}$ is gusset plates critical buckling load based on Thornton's method, and P_{BRB} is BRB compression strength.

2.3. Finite element modeling

The FE software ABAQUS was used to model the two steel frames with both the hinge and continuous beam. Unlike the cyclic loading used in the experiment, the frames were monotonically loaded. Then, the numerical models were calibrated with the envelope of the four experimental hysteretic loops. The monotonic loading is suitable to determine the gusset buckling capacity because the experimental BRBs exhibited non-deteriorating hysteretic loops (Dhakal 2021). The beam, columns, gusset plates, stiffeners, lug plates, and load plates were modeled using linear, finite-membrane-strain, reduced-integration, quadrilateral shell (S4R) elements (Figure 4). These elements exhibit good in-plane bending behavior with enhanced hourglass control and are efficient in simulating the bending behavior of thin plates (Dassault Systems, 2012).

The BRB components (core, concrete, and casing) were not explicitly modeled because it is computationally expensive, and the BRB's internal behavior is not the primary topic of this study. Therefore, BRBs were simulated using coupled wire beams, as shown in Figure 4. The interior wire beams had the

rectangular profile properties of the experimental BRB core. A second, exterior, wire beam was modeled with the geometric properties of the BRB restrainer casing to enhance the OOP core stiffness. The concrete and steel geometry of the casing was input as a steel-only component by using the modular ratio of steel and concrete, and the assumption of composite action.

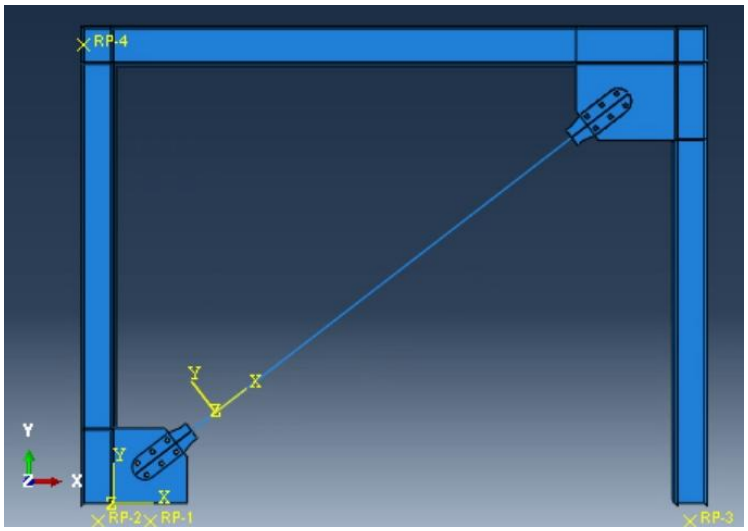

Figure 4. Representative ABAQUS Model of Frame 2b.

The material properties of the frame members corresponded to those of the experimental specimens. A bilinear material constitutive relationship was used for the steel beam, columns, and plates, with $F_y = 345$ MPa (50 ksi), $F_u = 448$ MPa (65 ksi), and engineering strain at failure $\varepsilon_u = 0.15$. For the BRB core material, $F_y = 290$ MPa (42 ksi), $F_u = 414$ MPa (60 ksi), and $\varepsilon_u = 0.15$. However, the BRB ultimate strain in the model was reduced to 0.03 to simulate the expected core strain corresponding to the ultimate core strength (Wang et al. 2019, Ibarra and Dhakal, 2022).

Regarding kinematic constraints, the frame columns were fixed at the base, and the beam-column connections were assumed as rigid. Given that the experimental frame was constrained against OOP translational displacement, the OOP displacement U3 in the numerical model was set to 0. Where boundary conditions were to be applied, the surfaces were kinematically coupled to reference points in all degrees of freedom, and the BCs were then applied to the reference points. A shell plate of the actuator plate size was attached to the left column to simulate the load applied by the actuator in the experiment (reference point RP-4 in Figure 4). Then, an in-plane compressive displacement was applied to the actuator plate, resulting in BRB axial compression forces that increased monotonically until failure of any BRBF component was detected in a pushover analysis. The general static step approach with non-linear geometry was used to apply the in-plane displacement. A maximum load step of 0.01 was used in the non-linear analysis, resulting in 3.81 mm (0.15 in.) incremental displacements, given that the total displacement was 381.0 mm (15.0 in.).

An initial imperfection was applied as a base state for static analysis, to simulate the OOP buckling behavior in the gusset plates. To define this imperfection, an elastic buckling analysis was carried out separately,

and the first mode shape of the gusset plate from this elastic analysis was used as the perturbed geometry for most realizations. The FE model OOP initial imperfection of Frame 2 was 5.1 mm (0.2 in.) at the center of the top large gusset plate, as measured in the experimental frame (Ibarra, 2017; Dhakal, 2021). Most of this imperfection was caused by misalignment of the gusset plate with respect to the beam-column centerline. A scale factor of 0.5 was used along with the first mode shape to achieve this initial imperfection in ABAQUS (Figure 5)1.

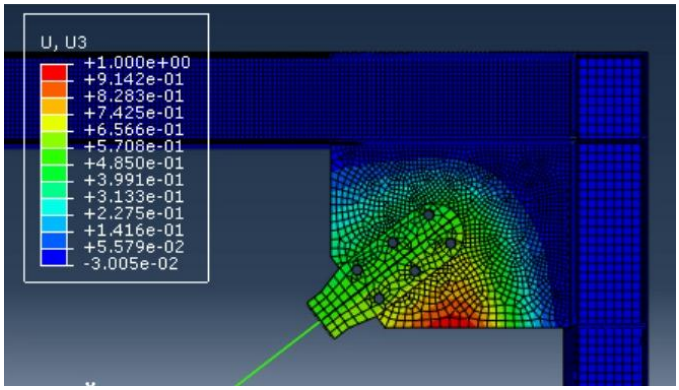

Figure 5. Contour of OOP Displacement in Top Large Gusset Plate for First Buckling Mode.

Several constraints were used for the connection of frame members in the FE model. As can be seen in Figure 6, the welded components in the experimental setup (e.g., beam-column interface, gusset-beam-column interface) were modeled as tie constraints to simulate the expected rigid connection. For the frames' bolted connections (i.e., splice in hinge beam connection and gusset-lug connection), the bolt effect was simulated by connecting the center of holes with a Multi-Point Constraint (MPC) rigid beam. The structural coupling was used between beam ends and corresponding hole edges in plates (Figure 7). Also, a surface-to-surface interaction was defined between lug and gusset plates using a hard contact along the contact planes, and a penalty contact friction factor of 0.6 was defined along the tangential direction. The gusset plates were defined as master surfaces, while lug plates were slave surfaces.

Kinematic coupling was used to assign BRB core and restrainer BCs (Figure 6), and it was defined along the members' length at each 152 mm (6 in), a distance selected after a sensitivity study showed that larger spacing may lead to core plate local buckling. The BRB degrees of freedom were restrained in the kinematic

[1] The imperfection cannot be applied in ABAQUS graphical user interface. Therefore, the following keyword was added in the static analysis.

*IMPERFECTION, FILE NAME= filename, STEP=1

1,0.5

The first number – "1"– in the second line represents the mode shape of interest. The second number – "0.5" – is the factor multiplying the displacement from the elastic analysis to achieve the desired magnitude of the imperfection at the reference point (middle of top gusset here). The perturbed geometry will act as the base state for static analysis, and the displacement calculated in the main or static analysis will be relative to this perturbed geometry

coupling, except in the axial direction, given that an un-bonding medium prevents the axial force transfer between core and restrainer in the actual BRB. Master nodes were assigned to the core and slave nodes on the restrainer. This interaction enhanced the core's buckling capacity by utilizing the stiffness of the restrainer when the load exceeded the buckling capacity of the core alone. The MPC beam simulated the connection between core and lug plates.

The core and restrainer were modeled with two-node linear beam in space elements (B31), whereas the rest of the members – including beam, columns, and plates – were modeled with four-node shell elements (S4R). The mesh sizes of the beam, column, and plate elements were approximately 12.5 mm (0.5 in.). A mesh sensitivity analysis showed that these sizes are a suitable compromise between accuracy and analysis time (Dhakal, 2021). The section forces in the beam elements were assumed to indicate the gusset plate load, based on force equilibrium.

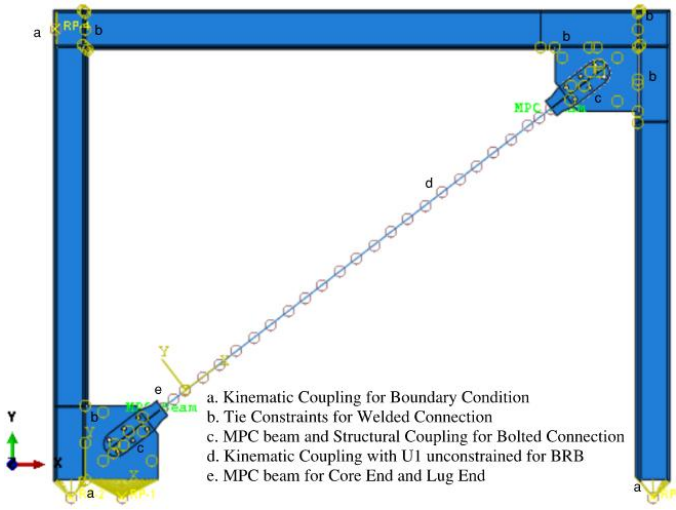

Figure 6. Interaction in FE Model.

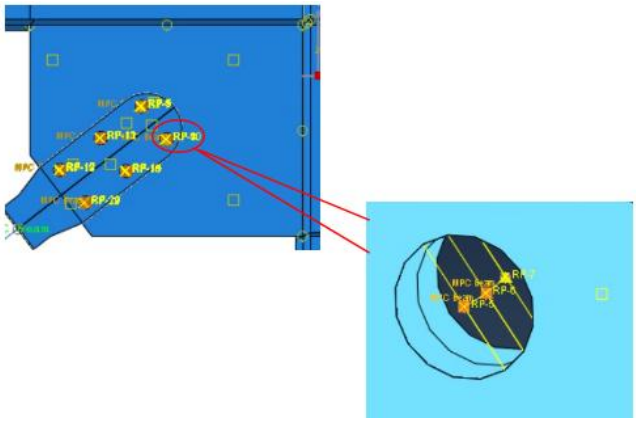

Figure 7 Bolt Modeling.

3. Results

3.1. Numerical evaluation of experimental tests

The numerical BRBF models were validated with the experimental results up to a lateral load of 830.8 kN (187.0 kips) in compression, which was the maximum load the actuator was able to deliver. The maximum load recorded in tension was 1,014 kN (228 kips), about 4% more than the BRB compression strength, P_{BRB}, computed with Eqn. 1. The experimental tests did not lead to overall frame failure at that load level, but after applying loading protocols that account for cumulative inelastic deformation, gusset plate damage was observed, including weld fracture and permanent plate deformation. To estimate the critical buckling load, pushover analyses were performed using the calibrated experimental models. Figure 8a presents the pushover curves for the frame in-plane load vs. drift at the beam centerline, Figure 8b shows the axial load - strain curves for the BRB steel core, and Figure 8c compares the experimental hysteresis and pushover curve for frames with large gusset plates and continuous beam. As observed, the experimental hysteresis is more flexible because it was first tested with a hinged beam, and some joints or connections could not reach the fixed or rigid boundary conditions used in the numerical simulation.

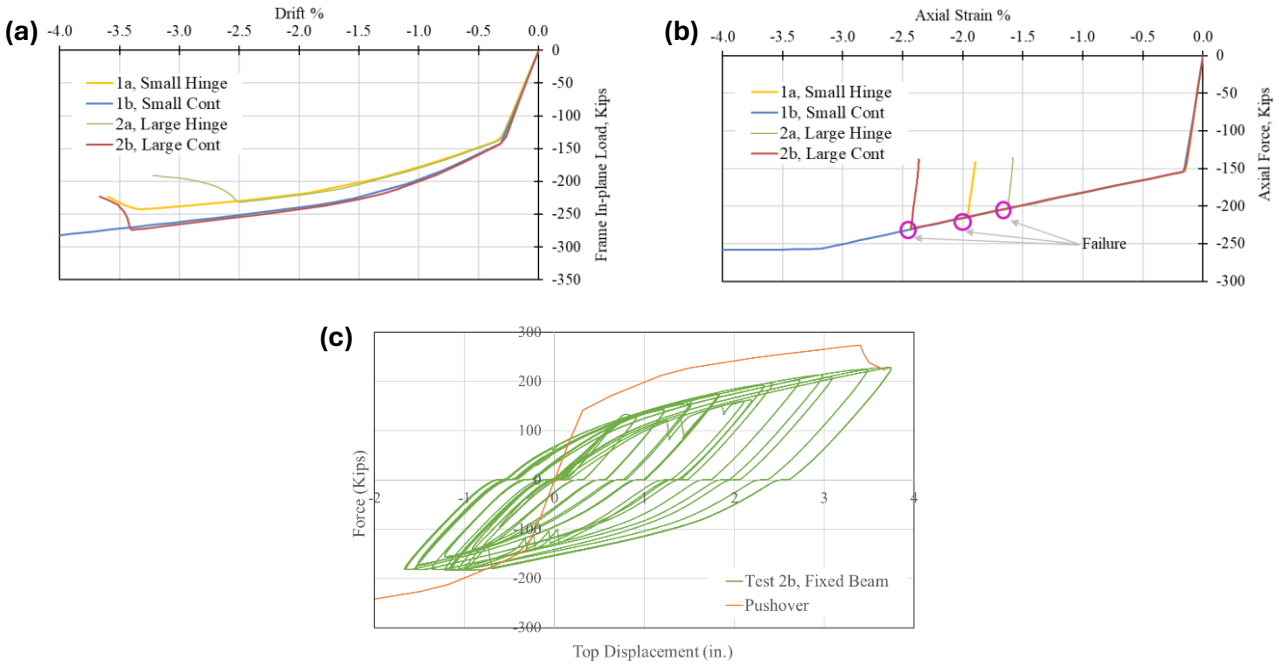

Figure 8. (a) Pushover Curve for Experimental Frames, (b) Core Axial Force Versus Axial Strain Relation for Experimental Frame Models, (c) Experimental Hysteresis and Pushover Curve for Frames with Large Gusset Plates and Continuous Beam [1 kip = 4.45 kN].

The FE analyses were performed until the load-deformation relationship reached its peak strength, and a softening loading path was detected, typically indicating buckling failure. For example, the maximum load reached in Frame 2b was 1,219 kN (274 kips) at a lateral drift of about $\Delta_{frame} = 3.4\%$ (Figure 8a). The associated buckling load in the BRB core was $P_{cr,FE} = 1{,}023$ kN (230 kips) at a core axial strain of 2.4% (Figure 8b). Typically, BRBs under cyclic loading experience failure at axial strain between about $\varepsilon_{core} = 1.5$

and 3.5% (e.g., Wang et al. 2019, Andrews et al. 2009). The BRB core axial strain obtained in the FE model was approximately in the middle of this interval. Also, the frame's drift, Δ_{frame}, was slightly higher than the expected drift with rigid frame components. For instance, for Frame 2b, $\Delta_{frame} = \varepsilon_{core}/\cos\theta$ = 0.024(100)/cos (36.9) = 3.0%, whereas the reported $\Delta_{frame} = 3.4\%$. The difference is attributed to the elastic deformation of the frame components, and fixed and rigid joint BCs that cannot be fully reached on the experimental tests.

Table 2 presents the critical load for the experimental frames as computed using FE models. The frame load at failure is $P_{L,FE}$, and corresponds to the lateral load applied in the displacement-controlled analysis at Point RP-4 in Figure 4. The $P_{L,FE}$ may be caused by several failure modes, such as gusset plate buckling, core fracture, and splice plate rupture, among others. Table 2 also includes the critical buckling load of the BRB core, $P_{cr,FE}$, which will be used in the rest of the study to obtain a direct comparison with Thornton's critical load, $P_{cr,\mathrm{T}}$.

Table 2. Analytical and Numerical Failure Prediction for Experimental Tests

Frame	Thornton $P_{cr,T}$ kN (kips)	Critical Load, FE			$P_{cr,T}/P_{cr,FE}$	Governing BC Failure Mode
		$P_{L,FE}$ Frame kN (kips)	$P_{cr,FE}$ Core kN (kips)	$\varepsilon_{cr,core}$		
1a	1201.0 (270.0)	1078.0 (242.3)	955.3 (214.8)	2.1%	1.26	Splice Plate Rupture *
1b	1201.0 (270.0)	1317.7 (296.6)	1139.6 (256.5)	3.2%	1.03	Core Fracture
2a	969.7 (218.0)	1030.1 (231.6)	902.0 (202.8)	1.6%	1.08	Top Gusset Buckling *
2b	969.7 (218.0)	1218.9 (274.0)	1023.0 (230.0)	2.4%	0.95	Top Gusset Buckling
* The overall controlling mode is BRB core failure, as $P_{cr,FE} < P_{cr,BRB} = 977$ kN						

As observed in Table 2, the $P_{cr,FE}$ of frames with hinge beams (1a and 2a) is about 10-20% smaller than that of their counterpart frames with continuous beams (1b and 2b, respectively). Thornton's method does not consider the frame action contribution and provides the same critical load for frames with a hinge or continuous beams. The $P_{cr,T}/P_{cr,FE}$ ratios show that Thornton's methodology overestimated the critical load in three of the frames. Regarding the gusset size effect, Table 2 shows that the $P_{cr,FE}$ of Frames 1a and 1b is approximately 6-10% higher than that of the corresponding frames with larger gusset plates (Frames 2a and 2b, respectively).

Table 2 also shows the FE model's failure modes. For Frames 2a and 2b, buckling of the large top gusset was the controlling failure mode (Figure 9). Frames with short guesset plates exhibited a different failure mode. In Frame 1a the beam's splice plate failed, whereas Frame 1b exhited core fracture, followed by buckling of the small top gusset plate. Note, however, that BRB boundary condition failure modes will take

place only if their capacity is less than $P_{cr,BRB} = 977$ kN (220 kips), a failure mode not detected in the FE models. As shown in Table 2, however, $P_{cr,FE} < P_{cr,BRB}$ for the two frames with hinges (Frames 1a and 2a). The use of a continuous beams in Frames 1b and 2b leads to a better stress redistribution, increasing $P_{cr,FE}$.

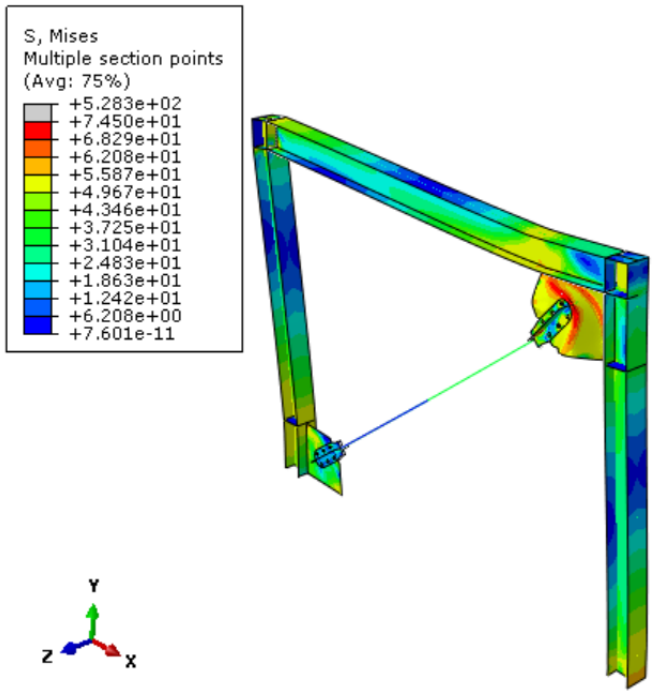

Figure 9. Large Top Gusset Plate Deformed Shape (Scaled up 2.5) of Frame 2b.

3.2. Parametric study

The only parameters that were varied in the experimental tests were the gusset plate size and the beam continuity. Then, to assess the effect of gusset plate parameter variation on BRBF response, the following study of frames with continuous beams addresses variations on the gusset plate length and thickness, BRB lug plate configuration, initial imperfection, and the mode shape used to represent this imperfection. Each evaluated parameter varies over a given interval, while the rest of the model parameters remain constant. The numerical study focuses on frames with continuous beams, as these were the experimental specimens tested into the nonlinear inelastic range.

The numerical models presented in previous sections for replicating experimental frames are the baseline models in the parametric study. The frame's nomenclature used in the rest of the paper is first introduced in Table 3. For instance, the model ID of the baseline frame is LG-3/8-CB-CLg-I.20-S1, indicating a large gusset plate (LG) of thickness 9.53 mm (3/8 in.), with a continuous beam (CB), BRB cruciform lug plates (CLg), an initial imperfection Δ_{imp}= 5.1 mm (0.2 in.) at the center of the gusset plate (I.20), an imperfection represented in the FE model with the first mode shape of the gusset plate (S1). This large initial imperfection of 5.1 mm (0.2 in.) is equivalent to l_{avg}/53, and it was mainly caused by a misalignment of the large gusset plate with respect to the beam-column centerline, with a minor contribution from plate distortion. The small gusset plate has about half the average length of the large gusset plate. Thus, an initial imperfection

Δ_{imp}= 2.54 mm (0.10 in.) was selected at the center of the gusset to keep the Δ_{imp}/l_{avg} ratio constant for the two gusset plate sizes, providing consistent and conservative results from the FE simulations.

3.2.1. Gusset plate thickness variation

The gusset plate thickness in the experimental frames was t_g = 9.53 mm (3/8 in.). To assess its effect on $P_{cr,FE}$, in this parametric study t_g varied from 6.35 to 12.70 mm (1/4 to 1/2 in.). The gusset thickness has an optimal design interval, given that very thin plates develop large stresses, whereas very thick plates may cause damage to adjacent members' webs (Palmer et al., 2013). A common upper limit for the gusset plate thickness is the 4/3 rule-of-thumb, in which the gusset cannot be thicker than 4/3 the lesser member web thickness. The experimental gussets plates were designed using t_g = 9.53 mm (3/8 in.), which complies with the 4/3 rule. In the parametric study, however, this rule was not met for the upper thickness limit t_g = 12.70 mm (1/2 in.).

Table 3 compiles the effect of thickness variation on $P_{cr,FE}$ critical load. The second column in this table is the Dowswell (2006) compact plate criterion, which states that buckling failure only needs to be checked if $t_g < t_\beta$. As can be seen, only two frames with large gusset plates and small thickess (t_g = 6.35 and 7.94 mm) are in this situation. The gussets of these configurations would be considered non-compact plates, and $P_{cr,T}$ would be computed with K = 1.0 (Dowswell, 2006). The rest of the configurations would have compact gusset plates, where yielding limit state is applicable and buckling capacity does not need to be computed.

As observed in Table 3, t_g can significantly modify $P_{cr,FE}$ and the failure mode. For instance, a gusset plate thickness reduction of only 1.588 mm (1/16 in.) from the original t_g, reduces the critical load by about 30%. Also, the $P_{cr,T}/P_{cr,FE}$ ratios in Table 3 show that $P_{cr,T}$ calculation with if K = 0.65 is reasonably close and conservative for $P_{cr,FE}$ for frames with large gusset plates. However, for some frames with small gusset plates the Thorton's method is slightly unconservative and $P_{cr,T}/P_{cr,FE}$ = 1.04, if Thornton's method is applied with K = 0.65 and l_{avg}. Increasing K to 1.0 would limit these $P_{cr,T}/P_{cr,FE}$ ratios to less than unity, although some configurations with large gusset plates would be significantly underestimated. For the frames presented in Table 3, however, $P_{cr,T}/P_{cr,FE}$ ratios slightly larger than the unity are not of concern, given the large imperfection considered in the gusset plates. Thus, Thorton's method with K = 0.65 and l_{avg} provides acceptable results.

The $P_{cr,T}/P_{cr,FE}$ ratio for three configurations is deemed not applicable (NA) because the frame failure is controlled by BRB failure. In addition, $P_{cr,T}$ in these cases is significantly larger than $P_{cr,FE}$, but these critical loads are not comparable as failure in the FE models is not due to gusset plate buckling, but stresses larger than core the stress at fracture.

The last column of Table 3 shows the failure mode obtained from the FE models. The gusset plate buckling controls for almost all cases where $t_g \leq$ 9.53 mm (3/8 in.). For cases with t_g = 12.70 mm (1/2 in.), the plate stresses exceeded the ultimate fracture limit for frames with small and large gusset plates, given that only a very rigid gusset plate can reach stresses closer to yield stresses. This behavior is evidenced in Figure 10a,

which presents the BRB core axial force-axial strain relationships for frames with large gussets of different plate thicknesses.

Table ¡Error! No hay texto con el estilo especificado en el documento.**.** Effect of Thickness Variation on BRBF Critical Load.

Model ID	t_g vs t_β mm (in.)	$P_{cr,T}$* kN (kips)		Core data		$\frac{P_{cr,T}}{P_{cr,FE}}$		FEM Failure Mode
		$K = 0.65$	$K = 1$	$P_{cr,FE}$ kN (kips)	ε_{cr} %	$K = 0.65$	$K = 1$	
LG-1/4-CB-CLg-I.20-S1	6.35<8.51 (0.25 <0.34)	449.3 (101.0)	204.7 (46.0)	498.2 (112.0)	0.1	0.90	0.41	Top GP buckling
LG-5/16-CB-CLg-I.20-S1	7.94<8.51 (0.31<0.34)	711.7 (160.0)	399.7 (89.9)	784.7 (176.4)	0.8	0.91	0.51	Top GP buckling
LG-3/8-CB-CLg-I.20-S1‡	9.53>8.51 (0.38>0.34)	969.7 (218.0)	650.9 (146.3)	1023.0 (230.0)	2.4	0.95	0.64	Top GP buckling
LG-1/2-CB-CLg-I.20-S1	12.70>8.51 (0.50> 0.34)	1467.9 (330.0)	1173.3 (263.8)	1139.0 (256.1)	3.2	NA	NA	Core stress > Fracture stress
SG-1/4-CB-CLg-I.10-S1	6.35>4.80 (0.25> 0.19)	725.1 (163.0)	564.8 (127.0)	699.6 (157.3)	0.6	1.04	0.81	Top GP buckling
SG-5/16-CB-CLg-I.10-S1	7.94>4.80 (0.31> 0.19)	965.3 (217.0)	823.6 (185.2)	924.4 (207.8)	1.8	1.04	0.89	Top GP buckling
SG-3/8-CB-CLg-I.10-S1‡	9.53>4.80 (0.38> 0.19)	1201.0 (270.0)	1074.5 (241.6)	1139.6 (256.5)	3.2	NA	NA	Core stress > Fracture stress
SG-1/2-CB-CLg-I.10-S1	12.70>4.80 (0.50> 0.19)	1654.7 (372.0)	1556.5 (349.9)	1131.6 (254.4)	3.1	NA	NA	Core stress > Fracture stress
* Thornton's critical load based on l_{avg} ‡ Baseline case								

Frames with thicker plates would fail due to other causes before gusset plate buckling occurred, such as fracture of the gusset plate, welding failure, and BRB steel core fracture, among others. The thinnest gusset plate of 6.35 mm (1/4 in.), however, exhibited plate buckling even before its core reached the inelastic interval. Figures 10b, 10c, and 10d show the Von Mises stress distribution for the 1/2, 3/8, and 1/4 in. thick gusset plates at the time of failure. As observed, the stresses in the 1/2 in. gusset plate reach the ultimate strength level at localized plate corners, without exhibiting a pattern associated to plate buckling failure. On the other hand, the 3/8 in. plate, and especially the 1/4 in. plate, exhibit large stresses over an extended

plate area, which are associated with large OOP plate deformations. Note that the stress distribution for the ¼" plate shows the elliptical band characteristic of plates reaching buckling failure.

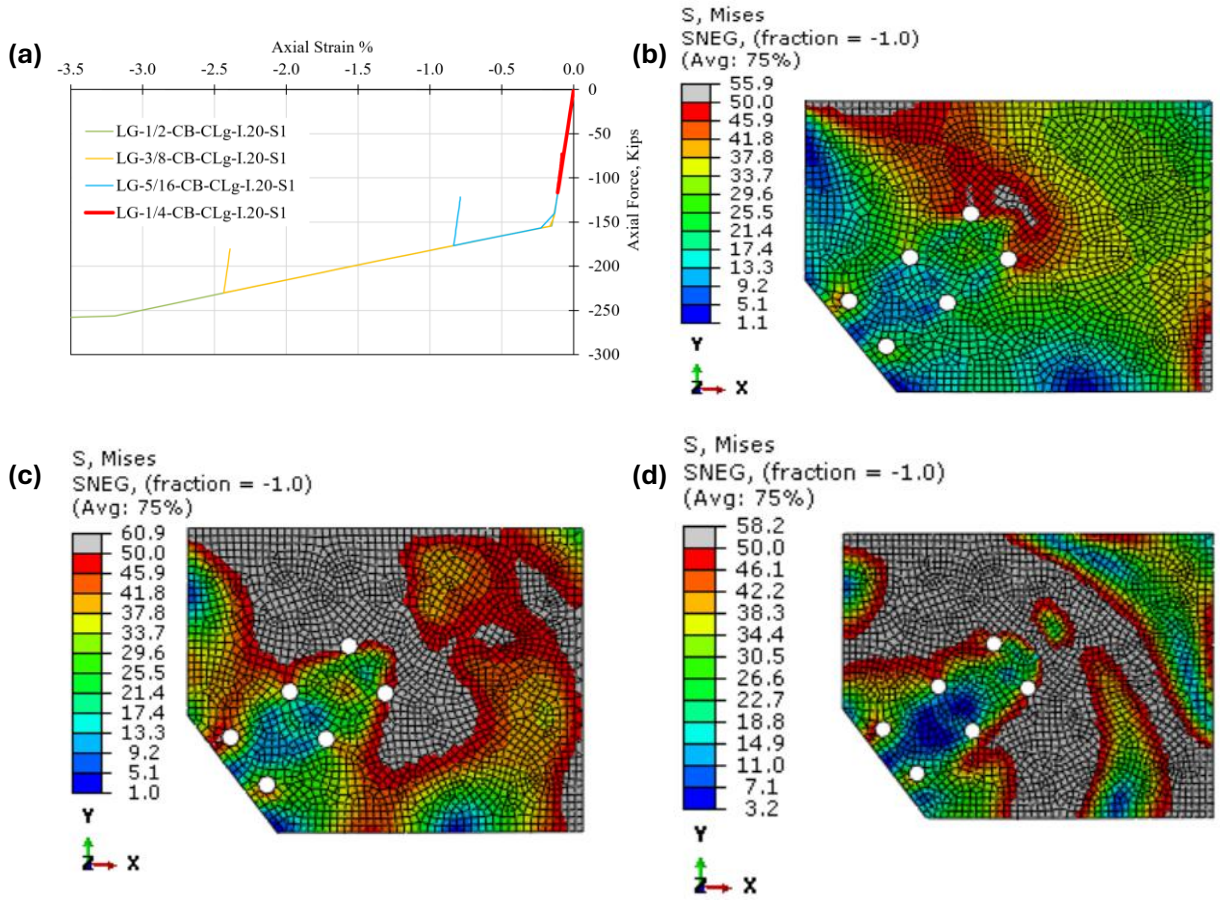

Figure 10. Large Gusset Continuous Beam Frames. (a) Core Axial Force - Axial Strain Relationships, (b)(c)(d) von Mises Stresses on a 1/2, 3/8, and 1/4 in. plate thickness, respectively. Units: 1 Kip = 4.45. kN, 1 ksi = 6.9 MPa.

The AISC (2016) recommends Thornton's critical load formulation in case the gusset plate is non-compact and the buckling load needs to be computed. If the Dowswell compact plate criterion is met, it is assumed the gusset plate can reach its yielding capacity. However, the FE models and Thornton calculations show that most of these assumed compact plates cannot reach their yield stress. For instance, the recommended Thornton's inelastic buckling calculations indicate the large gusset plate of the experimental frame LG-3/8-CB-CLg-I.20-S1 reaches critical stress at $F_{cr} = 0.75F_y$, i.e., a 25% stress reduction for a plate that is relatively large, but still is considered compact (the FE model predicts $F_{cr} = 0.79F_y$). Moreover, these calculations are based on the less conservative assumptions of $K = 0.65$ and l_{avg}. If the stress is computed with $K = 0.65$ and the central unbraced length l_1, $F_{cr} = 0.55F_y$. For $K = 1.0$ and l_1 the critical stress is only $F_{cr} = 0.25F_y$. Therefore, reasonable variations in the selection of K and the unbraced length lead to significantly different critical stresses. On the other hand, the experimental frame case SG-3/8-CB-CLg-I.10-S1 shows inelastic buckling on its small gusset plates, and $F_{cr} = 0.92F_y$ when

$K = 0.65$ and l_{avg} are used in the calculations. This is just an 8% load reduction from the compact plate capacity. Nevertheless, most of these presumed compact gusset plates experience some degree of stress reduction from the yield stress, and the critical buckling load should be computed for all cases.

3.2.2. BRB end lug plates configuration

The BRBs in the experimental tests included a cruciform shape at the end lug plates, with orthogonal plates oriented in the OOP direction, significantly increasing the bending rigidity in this orientation. There are, however, available BRBs that only include end plates oriented in the in-plane direction, or small orthogonal OOP plates. In these cases, the OOP rigidity of the endplates may be orders of magnitude lower than that of a similar BRB with cruciform endplates. This BRB design feature can modify the kinematic constraint at the end plate. Table 4 shows the critical load P_{cr} of FE models representing the experimental tests and similar models where the OOP plates were removed (i.e., no cruciform lug: nCLg). These models have a ratio Δ_{imp}/l_{avg} = 1/53, corresponding to gusset imperfections of 20 and 10 mm (I-20 and I-10) for large and small gusset plates, respectively. The results showed that for these models, the lack of a cruciform shape decreased the $P_{cr,FE}$ by almost 50%, and the gusset plates experienced buckling failure before the BRB yielded, changing the expected failure mode.

Table 4. End Lug Variation Results

Model ID	$P_{cr,T}$ $k = 0.65$ kN (kips)	Core data		K needed for Thornton	FEM Failure Mode
		$P_{cr,FE}$ kN (kips)	ε_{cr}		
LG-3/8-CB-CLg-I.20-S1	969.7 (218)	1023.0 (230.0)	2.4%	-	Top GP buckling
LG-3/8-CB-nCLg-I.20-S1	969.7 (218)	548.1 (123.2)	0.1%	1.12	Top GP buckling
LG-3/8-CB-CLg-I.050-S1	969.7 (218)	1154.1 (259.5)	2.4%	-	Top GP buckling
LG-3/8-CB-nCLg-I.050-S1	969.7 (218)	654.9 (147.4)	0.13%	1.00	Top GP buckling
SG-3/8-CB-CLg-I.10-S1	1201.0 (270)	1139.6 (256.5)	3.2%	-	Core Fracture
SG-3/8-CB-nCLg-I.10-S1	1201.0 (270)	630.7 (141.8)	0.1%	1.95	Top GP buckling
SG-3/8-CB-CLg-I.025-S1	1201.0 (270)	1184.0 (266.5)		-	Top GP buckling
SG-3/8-CB-nCLg-I.025-S1	1201.0 (270)	790.8 (178.0)	0.87%	1.61	Top GP buckling

To verify that the significant decrease in the buckling capacity of the non-cruciform models was not largely caused by large gusset plate imperfections, the analyses were repeated with a smaller ratio $\Delta_{imp}/l_{avg} = 1/200$, resulting in imperfections Δ_{imp}= 1.28 mm (0.05 in.) and 0.64 mm (0.025 in.) for large and small gusset plates, respectively. The results indicated that the buckling capacity of the non-cruciform models was still almost half the capacity of the models with cruciform shape. Table 4 also shows that the most significant effect of the lack of a cruciform shape was the reduction on the core strain at failure, ε_{cr}.

The large effect of OOP rigidity of BRB lug plates is not currently considered in standards and guidelines. Instead, Thornton's original approach considers $K = 0.65$, a factor only recommended for a fixed-fixed gusset plate end condition (Table C-A-7.1; AISC 2016), but used for all BRB end plate configuration. The procedure could be modified to incorporate this parameter variation by changing K, the unbraced length, or both parameters. In this study, it was decided to modify K, and leave l_{avg} unchanged, because it better reflects the physical phenomenon of OOP rigidity variation. The fifth column of Table 4 shows the K values needed to have $P_{cr,T} = P_{cr,FE}$, when using l_{avg}. From these results, effective length factors $K = 1.20$ and 2.10 are considered a good fit for large and small gusset plates with no lugs, respectively. These high Kvalues recognize that the rigidity of these BRB end plates cannot prevent OOP gusset displacements, and are close to AISC recommendations. For instance, for ideal columns, K =1.20 is the recommended value of a prismatic column fixed at one end and rotation fixed translation free at the other end (Table C-A-7.1; AISC 2016), whereas the recommended $K = 2.1$ corresponds to a column fixed at one end and free to rotate and translate at the other end. Therefore, the BRB end plate should not be considered a fixed end, if it does not include a cruciform configuration with a lug plate that provides sufficient OOP rigidity. Conservatively, $K = 2.1$ is recommended for BRB end plates that do not include OOP plates.

3.2.3. Top gusset plate initial imperfection variation

The previous FE analyses considered an initial imperfection for the large gusset plate Δ_{imp}= 5.1 mm (0.2 in.) at the center of the plate. For the small gusset plate, Δ_{imp}= 2.54 mm (0.10 in.) at the center of the gusset to keep the same ratio $\Delta_{imp}/l_{avg} = 1/53$ for small and large gusset plates. This section explores the sensitivity of BRBF capacity to variation on initial gusset plate imperfections. Table 5 shows the effect of Δ_{imp} on $P_{cr,FE}$ for gusset plate frames. As expected, $P_{cr,FE}$ increases as Δ_{imp} is reduced, and may modify the failure mode. For large imperfections, the small and large gusset plates exhibited buckling failure, whereas no buckling was reported for models with smaller imperfections, where core fracture was the governing failure. The gusset plate characteristics also played an important role. For frames with barely compact large gusset plates, a rather small imperfection $\Delta_{imp}/l_{avg} = 1/210$ triggered gusset plate buckling. On the other hand, for frames with small gussets, buckling of the plates only occur for a large initial imperfection $\Delta_{imp}/l_{avg} = 1/26$, which is almost eight times smaller than for large gusset plates that are barely compact.

The FE buckling load of the baseline case, $P_{cr,FE}$ is slightly larger than $P_{cr,BRB}$ = 977 kN, even for a gusset plate with a rather large imperfection $\Delta_{imp}/l_{avg} = 1/53$. For larger initial imperfections $P_{cr,FE} < P_{cr,BRB}$, but these conditions are unlikely to occur due to code limitations. Note that Thornton's method does not

include the effect of the initial imperfection on the critical buckling load calculation. Given the good behavior of gusset plates with large Δ_{imp}/l_{avg} and cruciform lug plates, quality assurance procedures should prevent unexpected plate buckling failure due to excessively large initial imperfections.

Table 5. Effect of Initial Imperfection on Gusset Plate Capacity and Failure Mode.

Model ID	Δ_{imp} mm (in.)	Δ_{imp}/l_{avg}	$P_{cr,FE}$, kN (kips)	$P_{cr,FEbase}/P_{cr,FE}$ kN (kips) *	Failure Mode
LG-3/8-CB-CLg-I.50-S1	12.70 (0.50)	1/21	884.5 (198.9)	0.86	Top GP buckling
LG-3/8-CB-CLg-I.40-S1	10.16 (0.40)	1/26	928.9 (208.8)	0.91	Top GP buckling
LG-3/8-CB-CLg-I.20-S1	5.08 (0.20)	1/53	1023.0 (230.0)	1.00	Top GP buckling
LG-3/8-CB-CLg-I.10-S1	2.54 (0.10)	1/105	1113.3 (250.3)	1.09	Top GP buckling
LG-3/8-CB-CLg-I.05-S1	1.27 (0.05)	1/210	1154.1 (259.5)	1.13	Top GP buckling
LG-3/8-CB-CLg-I.025-S1	0.64 (0.03)	1/420 †	No buckling failure up to 1137 kN (256 kips)		Core Fracture
SG-3/8-CB-CLg-I.50-S1	12.70 (0.50)	1/10	1056.8 (237.6)	1.10	Top GP buckling
SG-3/8-CB-CLg-I.40-S1	10.16 (0.40)	1/13	1107.3 (248.9)	1.05	Top GP buckling
SG-3/8-CB-CLg-I.20-S1	5.08 (0.20)	1/26	1156.0 (259.9)	1.00	Top GP buckling
SG-3/8-CB-CLg-I.10-S1	2.54 (0.10)	1/53 ‡	No buckling failure up to 1141.0 (256.5)		Core Fracture

* $P_{cr,FEbase}$ = 1023.0 (230.0) and 1139.6 (256.5) for frames with large and small gussets plates, respectively.

† Similar results for imperfections of $1/840, 1/1400,$ and $1/2100$.

‡ Similar results for imperfections of $1/105, 1/210, 1/420, 1/700,$ and $1/1050$.

3.2.4. Gusset Plate Shape to Represent Initial Imperfection

The initial imperfection of the FE models presented above is based on the gusset plate first mode shape. However, many different configurations may lead to the same imperfection at the center of the plate. In this section the FE models consider a deformed shape based on the second modal shape. As observed in Table

6, the effect of using the second mode shape for the initial imperfection, modifies $P_{cr,FE}$ by less than 5%, and the axial strains by approximately 10%. The use of the second mode shape for a large gusset-continuous beam resulted in buckling of the top gusset plate, but had a different deformed shape at failure compared to the first mode shape (Figure 11). For the frame with a small gusset plate with a continuous beam, the failure mode changed to buckling of the bottom gusset plate. This is an expected scenario, given that the average unbraced length of the bottom plate and small top gusset plate is very similar.

Table 6. Imperfection Shape Variations in Experiment Model

Model ID	t_g vs t_β mm (in.)	$P_{cr,T}$ kN (kips)	Core data		FEM Failure Mode
			$P_{cr,FE}$ kN (kips)	Axial Strain	
LG-3/8-CB-CLg-I.20-S1	9.53 > 8.51 (0.38 > 0.34)	969.7 (218.0)	1023.0 (230.0)	2.4%	Top GP buckling
LG-3/8-CB-CLg-I.20-S2			1065.7 (239.6)	2.7%	Top GP buckling
SG-3/8-CB-CLg-I.10-S1	9.53 > 4.80 (0.38> 0.19)	1201.0 (270.0)	1139.6 (256.5)	3.2%	Core Fracture
SG-3/8-CB-CLg-I.10-S2			1103.3 (248.0)	2.9%	Bottom GP buckling

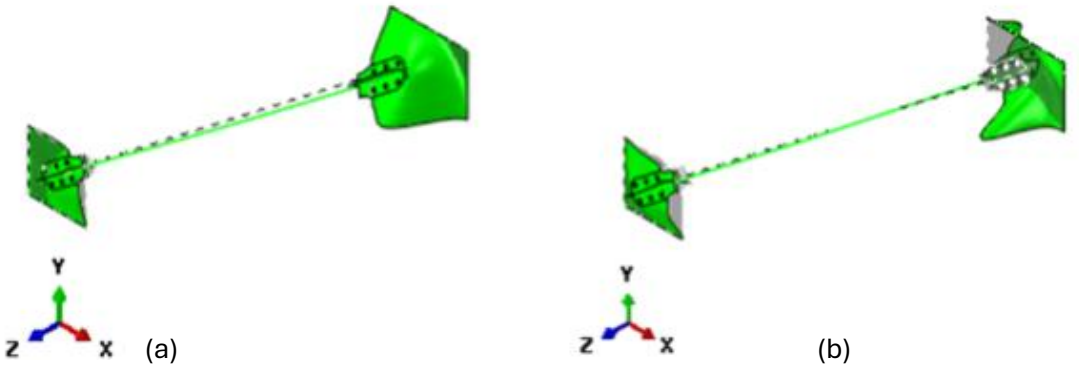

Figure 11. Buckling of Gusset Plates in Large Gusset Continuous Beam. (a) First Mode Shape (b) Second Mode Shape.

4. Conclusions

The performance of buckling restrained braced frames (BRBFs) is affected by BRB interaction with surrounding frame elements and bracing connections. Unlike conventional braces, BRBs can withstand large compression loads, which are then transferred to the gusset plates and frame components. Current design standards treat gusset plates as axially loaded members, without considering factors such as frame action, cruciform shape in BRB lug plates, and beam connection type. The FE software ABAQUS was used to study the effect of gusset plate length and thickness, cruciform shape in lug plates, as well as

imperfection magnitude and shape on BRBF capacity. The nonlinear performance of the BRBF models was validated with experimental results. The experimental tests were used to calibrate the FE models. The main findings are:

- The FE model realizations show that frames with the larger top gusset plate have a reduced capacity of 6-10 percent, compared to that of frames with a smaller top gusset plate.
- The critical load ($P_{cr,FE}$) for the numerical frames with hinge beams is 10-20% smaller than that of their counterpart frames with continuous beams. Thornton's method does not consider the frame action contribution and provides the same critical load for frames with a hinge or continuous beams.
- The gusset plate thickness significantly impacts its critical buckling load and failure mode. In the study, a thickness reduction of only 1.588 mm (1/16 in.) reduced the critical load by about 30%. However, if an appropriate design is implemented (as prescribed by AISC), the optimal gusset plate thickness interval is sufficiently large to avoid undesirable failure modes.
- The buckling capacity of gusset plates without cruciform BRB lug plates is reduced by almost 50%, due to the inability of these BRB end plates to prevent OOP displacements. The results indicate that an effective length factor $K = 0.65$ (fixed-fixed ends) is acceptable when computing the buckling capacity of BRBs having cruciform lug plates. However, $K = 2.1$ (fixed-free ends) is recommended for BRBs without cruciform lug plates.
- Based on the results of the gusset plates classified as compact, the gusset plate critical buckling load should be computed for all gusset plates, regardless of classification, in order to verify that the critical buckling load is larger than the BRB capacity.
- The modal shape used in the FE formulation to produce the initial imperfection at the center of the gusset plate has a small effect on the computed buckling load capacity.
- For BRBs with cruciform lug plates, plate buckling does not control as long as the imperfection is relatively small, but this criterion is different according to the gusset characteristics. In this study, the initial imperfection to average length (Δ_{imp}/l_{avg}) ratio leading to gusset buckling was almost eight times larger for frames with small gusset plates. Failure modes were highly dependent upon the magnitude of the initial gusset plate OOP imperfection, and it is recommended to control this condition with quality assurance protocols.
- The parameter with the largest influence on the BRBF seismic performance is associated to the cruciform lug plates. Several of the apparent contradictions in previous studies may be attributed to the design of the cruciform lug plates, and especially to the lack of them, in the BRB end plates configuration.

Acknowledgments

The authors thank the AISC Milek Fellowship and the University of Utah for funding this research. The authors are grateful to Saul Vazquez Colunga from The University of Canterbury, for his valuable guidance in the modeling process; and to Catherine Tucker and Mark Bryant for their contributions during the experimental tests used to verify and validate the numerical models. The findings, conclusions, or recommendations expressed in this publication are those of the authors and do not necessarily reflect the views of the sponsors.

References

AISC (American Institute of Steel Construction). 2012. Seismic Provisions for Structural Steel Buildings. AISC 341-10. One East Wacker Drive, IL: AISC

AISC (American Institute of Steel Construction). 2011. Steel Construction Manual.

AISC (American Institute of Steel Construction). 2016. Steel Construction Manual.

Andrews, B. M., Fahnestock, L. A., and Song, J. 2009. “Ductility capacity models for buckling-restrained braces.” Journal of Constructional Steel Research, 65(8), 1712–1720.

Ariyaratana, C., and Fahnestock, L. A. 2011. “Evaluation of buckling-restrained braced frame seismic performance considering reserve strength.” Engineering Structures, 33(1), 77–89.

Black Cameron J., Makris Nicos, and Aiken Ian D. 2004. “Component testing, seismic evaluation and characterization of buckling-restrained braces.” Journal of Structural Engineering, American Society of Civil Engineers, 130(6), 880–894.

Chou, C-C., and Chen, P-J. 2009. “Compressive behavior of central gusset plate connections for a buckling-restrained braced frame". Journal of Constructional Steel Research, 65, 1138–1148.

Chou, C.-C., and Liu, J.-H. 2012. “Frame and brace action forces on steel corner gusset plate connections in buckling-restrained braced frames.” Earthquake Spectra, Earthquake Engineering Research Institute, 28(2), 531–551.

Chou, C.-C., Liu, J.-H., and Pham, D.-H. 2012. “Steel buckling-restrained braced frames with single and dual corner gusset connections: seismic tests and analyses.” Earthquake Engineering & Structural Dynamics, 41(7), 1137-1156.

Daniels M. 2011. “Towards characteristic overstrength curves for buckling restrained braces.” Proc., Annual Convention of the Structural Engineers Association of California 2011, 69-73. Las Vegas

Dassault Systems 2012. “Abaqus Unified FEA”. Dassault Systems

Dassault Systems.2019. “Abaqus FEA.”

Dhakal, P (2021). “Effect of Buckling Restrained Brace (BRB) Boundary Conditions on the Seismic Resilience of Braced Frames.” Master of Science Thesis, The University of Utah. August 2021.

Dowswell, B. 2006. “Effective length factors for gusset plate buckling." Engineering Journal, 43(2), 91–101.

Ibarra, L. (2017) “Effect of Buckling Restrained Brace Boundary Conditions on the Seismic Resilience of Braced Frames: Status Report." Presented to American Institute of Steel Construction Committee, San Antonio, TX. 2017.

Ibarra L, and P Dhakal (2022) "Effect of Cruciform Lug Stiffeners on the Seismic Performance of Buckling Restrained Braced Frames." 12th National Conference on Earthquake Engineering, Salt Lake City, UT. 2022.

Lin, M.-L., Tsai, K.-C., Hsiao, P.-C., and Tsai, C.-Y. 2005. “Compressive behavior of buckling-restrained brace gusset connections." Proc., First International Conference on Advances in Experimental Structural Engineering, Advances in Experimental Structural Engineering (AESE).

Mahin, S. A., Uriz, P., Aiken, I., Field, C., & Ko, E. 2004. “Seismic performance of buckling restrained braced frame systems." Proc., Thirteenth World Conference on Earthquake Engineering, Vancouver, Canada.

Muir, L. S., and W. A. Thornton (2014). “Vertical bracing connections–Analysis and design,” Steel Design Guide 29, American Institute of Steel Construction, Chicago, IL.

Okazaki, T, T Hikino, and K Kajiwara. 2012. “Out-of-plane stability of buckling restrained braces." 15th World Conference in Earthquake Engineering, WCEE. Lisbon 2012.

Prinz, G. S., Richards, P. W., and Fremming, S. 2008. “Seismic response of buckling-restrained braced frames with beam splices." Proc., Fourteenth World Conference on Earthquake Engineering.

Roeder, C. W., Lehman, D.E., and Chistopulos, A. 2006. “Seismic performance of special concentrically braced frames with buckling restrained braces." Proc. 8th U.S. National Conf. on Earthquake Engineering, San Francisco, CA, Paper No. 1503.

Sabelli, R., Mahin, S., Chang, C. 2003. “Seismic demands on steel braced frame buildings with buckling-restrained braces." Engineering Structures, 25(5). https://doi.org/10.1016/S0141-0296(02)00175-X.

Sheng, N., Yam, C. H., and Iu, V. P. 2002. "Analytical investigation and the design of the compressive strength of steel gusset plate connections." Journal of Constructional Steel Research, 58, 1473-1493.

Kersting, R.A., L.A. Fahnestock, W.A. Lopez (2015) " Seismic Design of Steel Buckling Restrained Braced Frames. A Guide for Practicing Engineers." ATC. NIST GCR 15-917-34. September 2015.

Takeuchi, T., Kasai, K., Midorikawa, M., Matsuoka, Y., Asakawa, T., Kubodera, I., Kurokawa, Y., Kishiki, S., and Ando, H. 2008. “Shaking table test using E-Defense multipurpose test bed.” 14th World Conference on Earthquake Engineering, Beijing, China, October 12-17, 2008.

Takeuchi, T., H. Ozaki, R. Matsui, F. Sutcu (2014). "Out-of-plane stability of buckling restrained braces including moment transfer capacity." Earthquake Engineering Structural Dynamics, 43(6), 851-869.

Thornton, W. A. 1984. "Bracing connections for heavy construction." Engineering Journal, Third Quarter, 139-148.

Thornton, W. A., and Lini, C. 2011. "The Whitmore section: how to use the Whitmore method for tension and compression strength checks." Modern Steel Construction.

Tsai, K.-C., and Hsiao, P.-C. 2008. "Pseudo-Dynamic test of a full-scale CFT/BRB frame - part II: seismic performance of buckling-restrained braces and connections." Earthquake Engineering & Structural Dynamics, 37(7), 1099-1115.

Wang Y, L Ibarra, and C Pantelides. 2016. "Seismic retrofit of a three span bridge with buckling restrained braces." J. Bridge Engineering, 21(11), 04016073. https://doi.org/10.1061/(ASCE)BE.1943-5592.0000937.

Wang Y, L Ibarra, C Pantelides (2017) “Effects of Ground Motion Incidence Angle in Reinforced Concrete Skewed Bridge Retrofitted with Bucking Restrained Braces.” Structures Congress 2017, Paper 1457. Denver Co., April 6-8, 2017.

Wang Y, L Ibarra, C. Pantelides. 2019. "Collapse capacity of reinforced concrete skewed bridges retrofitted with buckling-restrained braces." Journal of Engineering Structures. https://doi.org/10.1016/j.engstruct.2019.01.033.

Watanabe, A. 1989. "Properties of brace encased in buckling-restrained concrete and steel tube," Proc., Ninth World Conference on Earthquake Engineering.

Westeneng B, C-L Lee, G MacRae, and A. Jones. 2017. "Out-of-plane buckling behavior of BRB gusset plate connections." 16th World Conference in Earthquake Engineering, WCEE, Paper 1419. Chile 2017.

Westeneng B, C-L Lee, G MacRae (2015) "Early Failure of Gusset Plates in Buckling Restrained Brace Frames." Steel Innovations Conf. 2015." Auckland, NZ. Sept. 2015.

Wigle, V. R., and Fahnestock, L. A. 2010. "Buckling-restrained braced frame connection performance." Journal of Constructional Steel Research, 66(1), 65-74.

Williams, G. C., and Richard, R. M. 1996. “Analysis and design of large diagonal bracing connections.”Structural Engineering Review,8,1–27.

Zaboli, B., G. Clifton, K. Cowie (2018). "BRBF and CBF gusset plates: Out-of-plane stability design using a simplified Notional Load Yield Line (NLYL) method." SESOC Journal, 31(1), 64.